Al-Mustansiriyah Journal of Science
ISSN: 1814-635X (print) 2521-3520 (electronic)

ORIGINAL ARTICLE *OPEN ACCESS*

Diagnosis of a Severe Dust Storm Event over Iraq

Sama K. Al-Dabbagh

Department of Atmospheric Sciences, College of Science, Mustansiriyah University, Iraq

CORRESPONDENCE
Sama K. Al-Dabbagh
sama.atmsc@uomustansiriyah.edu.iq

ARTICLE INFO
Received: May 08, 2025
Revised: June 18, 2025
Accepted: June 28, 2025
Published: June 30, 2025

ABSTRACT: ***Background:*** *Iraq experienced a severe dust event that occurred in mid-May 2022, disrupting daily life with adverse health impacts.* ***Objective:*** *This study aims to investigate the triggering weather systems, and examine the variations in meteorological factors during the event with a specific focus on Basrah station in southern Iraq.* ***Methods:*** *Ground-based meteorological observations and satellite imagery. In addition to the atmospheric composition forecast data from the copernicus atmosphere monitoring service (CAMS), including meteorological and optical properties for different levels. Applying statistical evaluations for CAMS data against observed data, including correlation coefficients, coefficient of determination, and error metrics (MBE and MAE).* ***Results:*** *The dust event was driven by a deep upper air cut-off low over the eastern Mediterranean region, coinciding with a southern intrusion of the polar jet stream. This situation led to baroclinic instability and the developing frontal cyclonic system over southern Turkey, Syria, Jordan, western Iraq to northern Saudi Arabia. Satellite images showed dense dust clouds swept and transported towards the east and southeast due to the front passage, which is simulated well in the CAMS model with a value exceeding 2.5 of optical depth. In Basrah station, the dust event led to a notable reduction in visibility, lower temperature by 4° C, and surface solar radiation of 15%. Wind speed, extinction coefficient, and humidity levels increase by about 2.2, 2, and 1.4 times respectively. 12% reduction in boundary layer height during daytime hours of a dust event, and an 8% increment during nighttime. The statistical assessment shows a strong correlation for temperature and humidity, moderate for wind speed, and weak for wind direction. The model overestimates temperature and wind direction, while underestimating humidity and wind speed. Errors are low for most variables but notably higher for wind direction.* ***Conclusions:*** *The May 2022 dust event was driven by a deep frontal cyclone, reaching central and southern Iraq, in which Basrah station witnessed reduced visibility, lower temperature and solar radiation, and increased wind speed, humidity, and extinction coefficient. Boundary layer height decreased during the day and rose at night, highlighting the atmospheric instability during the event.*

KEYWORDS: *Dust storms; CAMS; Dust RGB Imagery; Cold Front; Environment*

INTRODUCTION

Mineral dust is a key component of primary aerosols, and with sea salt, it is considered the most abundant aerosol by mass. Dust aerosols are mainly emitted from natural sources. It can be transported to long distances of thousands of kilometers as well as reaching up to high levels in the atmosphere according to its size and vertical mixing [1]. Being a PM source, the dust has negative wide effects on various aspects [2], such as human health [3]–[5], transportation sectors [6], and marine and terrestrial ecosystems [7]. Additionally, it plays a crucial role in cloud microphysics and the atmospheric radiative budget [8]–[10]. Dust can affect the greenhouse gas concentration and lifetime such as O_3 due to its contribution in the uptake and the release of some trace gases through heterogeneous interactions on dust surfaces. Those reactions are affected by meteorological conditions such as the relative humidity and the sunlight in addition to the shape and the morphology of the

dust particles [11], [12]. Middle East region contributes about 15-20 % of the global dust emission rate because it has many active dust sources [13]. Whilst, the Iraqi lands comprise significant dust sources, mainly in the alluvial plain and the western plateau. In addition to the border regions of Iraq with Syria, Saudi Arabia, and Iran [14], [15]. Due to climate change, there has been an increase in the frequency and intensity of Sand and Dust Storms (SDS) in the last two decades over the alluvial plains of Iraq and the Arabian Peninsula [16]. Dust particle emission is affected by wind speed, soil moisture, and vegetation type [17], [18].

From a synoptic-scale perspective, there are two types of atmospheric conditions forming large pressure gradients, generating high wind speed, and thus leading to episodic dust events in this region: summer Shamal and frontal systems. Shamal involves a high-pressure system extending from the Mediterranean to the northern Arabian Peninsula and Iraq, coinciding with Low pressure over the southern Arabian Peninsula and Iran. Frontal dust occurred mostly in spring, with similar pressure systems but with mutual and different locations of high and low [19]. Dust storms can occur locally such as Haboobs, as a result of thunderstorm downdrafts in desert regions [6], [20]. In addition to the enhancing role of the tropical atmospheric river in the maintenance of the low-pressure system, and the associated convective currents, leading to dust emission [21].

The rising frequency of dust events in recent years, and their significant impacts have led to a heightened interest in scientific studies on different aspects. For instance, the role of synoptic-scale systems [22]–[24], and the mesoscale (Haboob) systems [25], [26]. The identification of primary dust sources in Iraq and the region [14], [27], and the spatiotemporal distribution [28]. Other studies utilized numerical prediction models to simulate dust events such as WRF-CHEM [29], BSC-DREAM8b model [30], [31], and Trajectory and Dispersion Models such as HYSPLIT model [32], [33]. This study aims to diagnose the trigger behind the mid-May 2022 severe dust event through a synoptic analysis and investigate the change in meteorological factors during the event at Basrah station. The analysis utilizes ground-based METAR observations, atmospheric composition forecasts from the Copernicus Atmosphere Monitoring Service (CAMS), and satellite data from SEVIRI Dust RGB imagery.

MATERIALS AND METHODS

Iraq is located in southwestern Asia to the northwest of the Arabian Peninsula, between latitudes 29 ° 5 ′and 37 ° 22 ′ North and between longitudes 38 ° 45 ′and 48 ° 45 ′East with four main physical parts of different climates as follows: Alluvial plain and the desert plateau of hot desert climate, the mountainous range of Mediterranean climate and the terrain region of a Steppes Climate [34]. To investigate the meteorological drivers behind the dust event, a comprehensive synoptic analysis was conducted at both upper and surface atmospheric levels. This approach along with Satellite images allowed for tracing the dust plume from sources through its transport pathway across the region. Particular attention was given to meteorological variations during the event, focusing on Basrah station, where conditions were closely monitored. In addition to a statistical evaluation of the used modeled data. Thus, the following data were used:

Atmospheric Composition Forecast Data

Gridded data of global atmospheric composition forecasts from the European Center for Medium-Range Weather Forecasts (ECMWF) Copernicus Atmosphere Monitoring Service (CAMS) were used. Although reanalysis data, on the whole, is considered more accurate, forecast data is useful for analyzing short-term case studies. Moreover, CAMS forecast data includes some variables such as boundary layer height and the extinction coefficient which are not available in reanalysis datasets. For this reason, CAMS forecast data is utilized in this study.

The case study period is from 14-19 of May 2022, at 3h intervals with a spatial resolution of 0.4°x0.4°. CAMS produces analyses and forecasts globally by the Integrated Forecasting System of the ECMWF (IFS) which incorporates the latest modeling for both meteorology and atmospheric composition along with the data assimilation of satellite products. The system generates 1-h and 3-h intervals of predicted data for single-level and multi-level respectively at 0000 and 1200 UTC twice a day for up to five days forecast. The atmospheric compositions and meteorological variables have a spatial resolution of approximately 40 km horizontally and 137 levels vertically, from 2015 to the present [35]. Bilinear interpolation for CAMS data variables was implemented to determine the Basrah station based on the spatial information (longitude and latitude) using the CDO (Climate Data Operators) module (remapbil) [36]. Table 1 recapitulates the meteorological and pollutant forecasting variables used in this study.

Table 1. Meteorological and pollutants forecasting variables and their units of CAMS data

The Level of the Variable	Meteorological Variables	Pollutants Variables
Single level	Boundary layer height (m)	Total aerosol optical
	Total cloud cover (0 - 1)	depth (AOD) at 550nm
	10 m u and v components of wind (m/s)	
	Mean Sea Level Pressure (hPa)	Dust aerosol optical
	2m temperature and dew point (K)	depth (DOD) at 550nm
	Surface solar radiation downwards (J/m^2)	
Multi-level at the lowest model level (L137)	Aerosol extinction coefficient at 532 nm (1/m)	
Pressure level	Geopotential height (m) at 500 hPa	
	u and v component of wind (m/s) at 300 hPa, and 850 hPa	
	Temperature and dewpoint at 850 hPa (K)	

Ground-Based Meteorological Observations

In order to investigate the change in weather conditions during the dust event, and assess CAMS data, observations from the Meteorological Aerodrome Report (METAR) for Basrah station (ORMM) (30.517° N, 47.783° E) are used. It is one of the METAR stations within the Automated Surface Observing System ASOS was included. It offers visibility and some other meteorological parameters which is vital for the investigation of the mean atmospheric weather conditions in Basrah. This station, positioned in a downwind location, represents an ideal case study for testing the variations in meteorological factors during dust events. The meteorological parameters include visibility, surface temperature, and dew point at 2m, wind speed, and direction at 10m obtained from Basrah station were used in this study [37]. Based on visibility decoding, the type of weather phenomena significantly related to dust events or when there are no significant weather phenomena (meaning that Ceiling And Visibility OK (CAVOK)) are determined [38].

SEVIRI Dust RGB Satellite Data

In order to detect the dust plume and track its evolution during day and night hours, Dust RGB images of the Meteosat Second Generation (MSG) Spinning Enhanced Infrared and Visible Imager (SEVIRI) are used. The Dust RGB product is generated by a composite of three channels (IR12.0–IR10.8 (Red), IR10.8–IR8.7 (Green), and IR10.8 (Blue))[39].

RESULTS AND DISCUSSION

The Trigger of Dust Event

May 2022 witnessed a series of severe dust events in Iraq and some other countries in the Middle East. The meteorological stations recorded a spike in the occurrence of blowing dust, and mild, moderate, and severe dust storms [40].

The dust episode from 15-18th of May is the eighth event to hit Iraq since April this year, disturbing daily life, and sending thousands of people to hospitals [41].

To reveal the dust emission trigger, a synoptic analysis is conducted, and a look back at about 48 hours before the dust event outbreak is necessary. On May 14 at 12 UTC, 500 hPa geopotential height and 300 hP wind speed charts show a pronounced upper air cold trough with a cut-off low of 5710 gpm centered at ~25°E over the eastern Mediterranean, progressing eastward, coinciding with a strong wind (polar jet stream) exceeding 100 kt on its right side. The jet stream shows significant meandering which refers to wind speed oscillations, reflecting a southward intrusion of the polar jet stream, starting to initiate the mid-latitude depression (See Figure 1a).

After 24 hours, the Cut-Off Low developed into an open wave, noticing the convergence of geopotential height lines in the wave, which refers to the deepening of the low-pressure system (Figure 1b), leading to a state of baroclinic instability, forming a deep frontal cyclonic system, spans over southern Turkey, Syria, Jordan, western Iraq to northern Saudi Arabia (red shading region in Figure 1c).

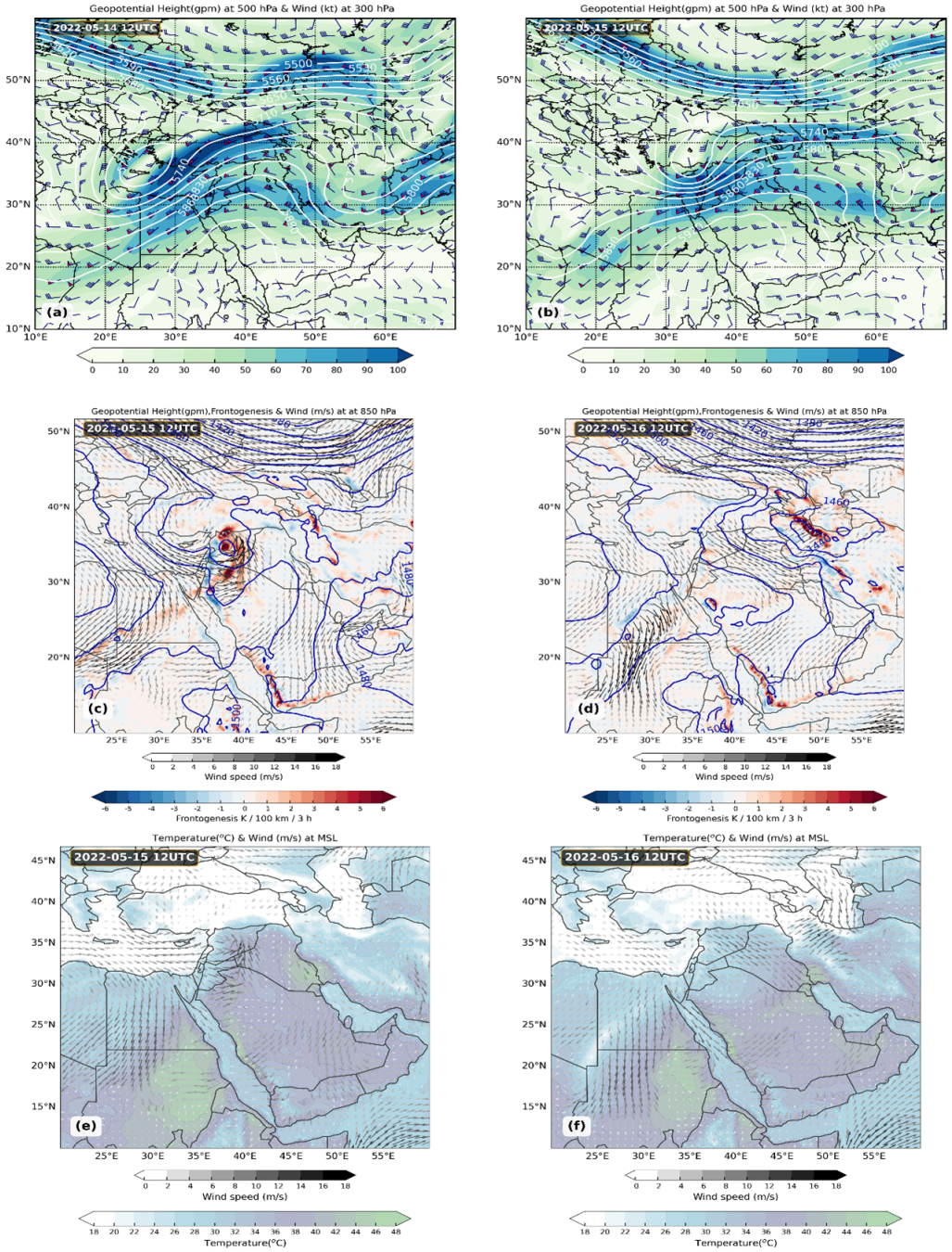

Figure 1. The synoptic atmospheric conditions: (a) & (b) the geopotential height (gpm) at 500 hPa and wind speed (shaded, Knot) at 300 hP on the 14th and 15th of May at 12 UTC, (c) & (d) geopotential height (gpm), wind speed (m/s), and the Frontogenesis (shaded, K/100 km/3h) at 850 hPa on 15th and 16th of May at 12 UTC, (e) & (f) Temperature (shaded, °C) and wind speed(m/s) at the MSL on 15th and 16th of May at 12 UTC.

 DOI: https://doi.org/10.23851/mjs.v36i2.1686

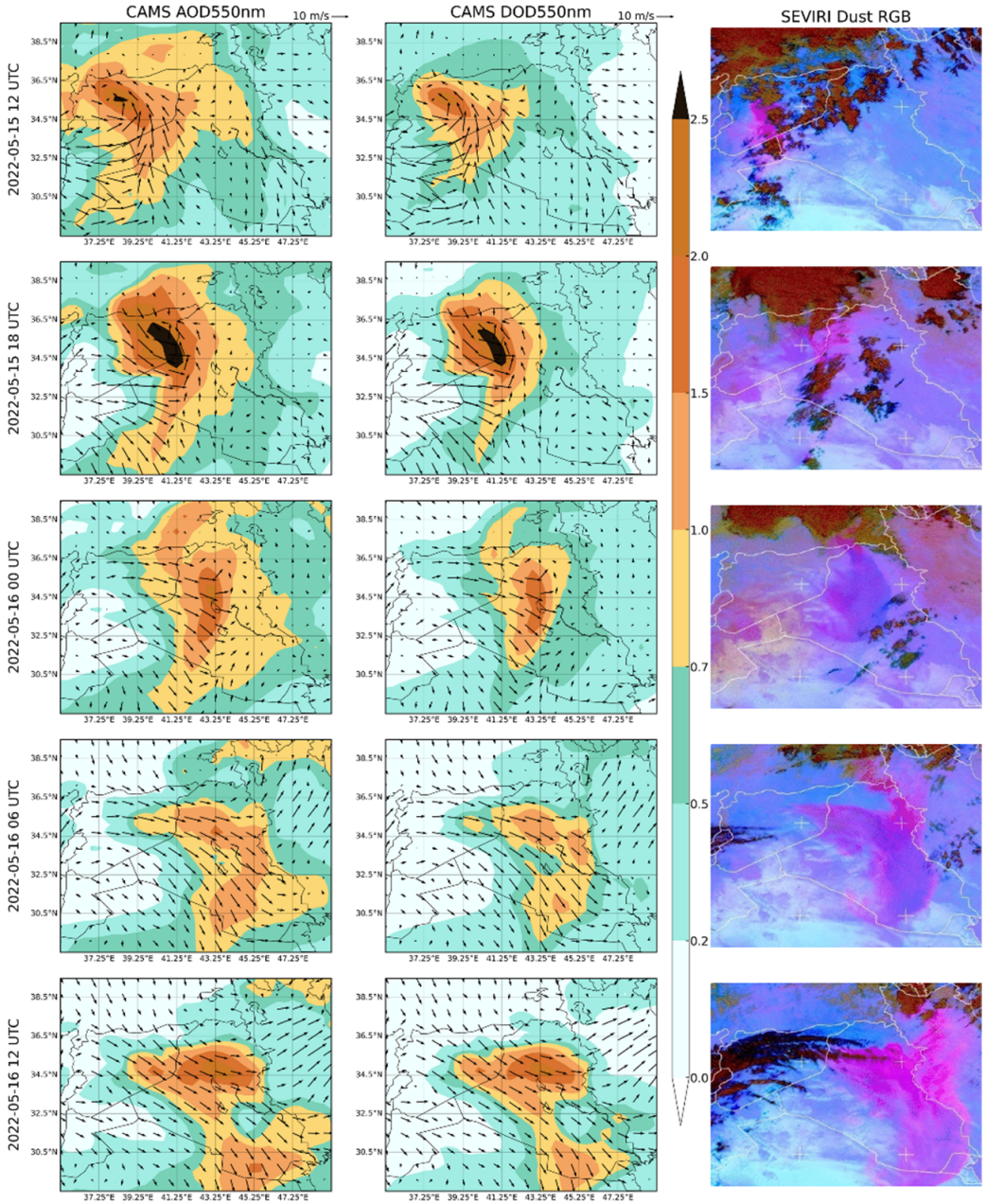

Figure 2. The development of the dust event with left columns: CAMS AOD at 550nm and 10 m wind at (m/s), middle columns: DOD at 550nm and 10 m wind at (m/s), and right columns: SEVIRI Dust RGB satellite image on 15th May at 12, 18 UTC and 16th May at 00, 06, 12 UTC 2022 respectively

At the surface, the descending cold air led to the form of a surface cold front over the aforementioned dry regions of deteriorating soil conditions with northwesterly wind (Figure 1e). The rapid cold air advection behind the front provoked sand and dust, forming a dense cloud on May 15 at 12 UTC as seen in satellite images (Figure 2). The plume is simulated well in both CAMS AOD and DOD with values over 1.5, and it is seen also in the SEVIRI dust RGB image (pink color). In the next few hours, AOD and DOD reached more than 2.5, as shown in Figure 2, indicating the severity of the dust plume.

Due to the northwesterly wind resulting from the frontal systems, the dust plume swept southeast on May 16, invading many provinces in central Iraq. It moved further to the east and the southeast, filling the sky with sand and suspended dust (Figure 2). Meanwhile, the advancing cold front reached Basrah station by 12 UTC (figures 1d and 1f), with a large temperature gradient, generating strong horizontal pressure gradients, and thus high wind speeds of about 20 m/s (~40 knots) near 900 hPa.

This level represents the residual layer that appears at Basrah station in the late hours and early hours of May 16 and 17 respectively (Figure 3). Wind speeds were lower at the surface (stable layer) due to friction. This situation caused wind shear and strong gusts, and thus, the boundary layer height has increased as shown in Figure 4a. The dust episode ended after the frontal passage on the late evening of May 17.

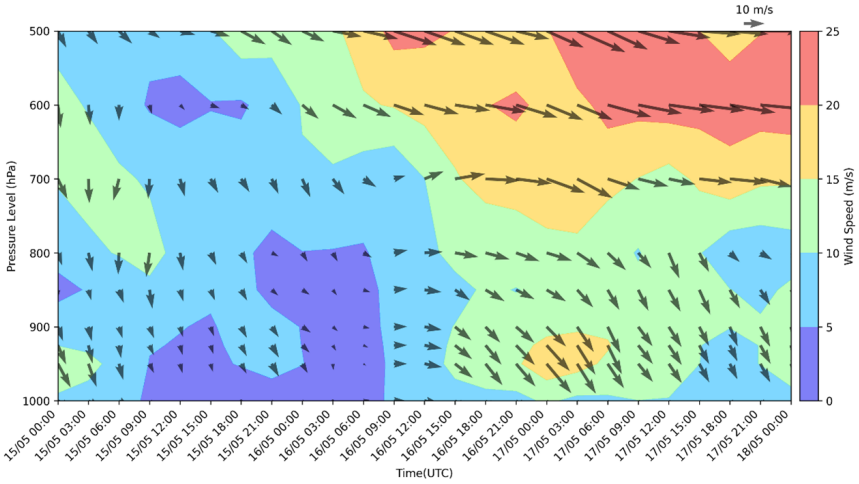

Figure 3. The temporal variation of the horizontal wind profiles from 1000 hPa to 500 hPa with shaded color representing wind speed (m/s)

The Meteorological Conditions at Basrah Station

Based on METAR observations at Basrah station, the selected clear weather interval or "before the dust event" is considered as May15-16 from 00:00 to 12:00 UTC respectively, highlighted in light blue shading (Figure 4), with visibility between 8000-10000 meters. While "during dust event" interval is from May 16-18, 12:00 to 00:00 UTC respectively. Thus, the comparison between those two intervals will help investigate changes in meteorological conditions.

During the dust event interval (Figure 4e), visibility sharply deteriorated on May 16, coinciding with a high wind speed of 12 m/s. By 15:00 UTC, it dropped to 100 m, indicating a dust storm (light reddish shading) with a wind speed of 10 m/s. On May 17 at 6:00 UTC, visibility improved to 600 m with a lower wind speed of 7 m/s, indicating widespread dust (orange shading). Later, it reached 1500 m at 12:00 UTC, with wind speed rising to 12 m/s, before the day ended with widespread dust and visibility around 7000 m with a lower wind speed of 7m/s, marking the end of the dust event.

On May 17 according to METAR data, the maximum observed temperature was lower by about 4 °C compared to May 15. While relative humidity dropped before the dust event in the early hours of May 16, compared to the previous day, but increased during dust conditions to 1.4 times on average (Figure 4a). This increment might be attributed to the thermodynamic effect of lower temperature. During the dust event, the wind is westerly to northwesterly (Figure 4c). It speeded up to 2.2 times on average during dust events compared to clear conditions (Figure 4b), evoking and transferring more dust from the source regions.

CAMS data showed a 12% reduction in boundary layer height (BLH) during daytime hours from 09:00 to 15:00 UTC within the dust episode compared to clear condition (Figure 4a). This reduction is attributed to lower temperatures due to cold front advection, and the scattering of solar radiation by dust particles. Additionally, the presence of clouds on May 17 further reduced surface solar radiation (Figure 4d). The maximum reduction of surface solar radiation reached about 15% at 03:00 UTC. However, BLH was significantly higher during the late evening and early morning hours of the dust event as explained earlier, reaching an 8% increase at 21:00 UTC compared to clear conditions.

The low observed visibility corresponds to a higher aerosol extinction coefficient compared to clear weather (2 times on average), due to the attenuation by dust particles.

The Statistical Assessment of CAMS Data

Both CAMS and METAR data showed almost similar patterns in the variation of temperature, relative humidity, wind speed, and direction (Figure 4 a,b,c). A statistical assessment of the performance of the CAMS data against METAR observed data is conducted for May, that summarized in Table 2. The metrics indicate a strong positive linear correlation coefficient (R) (0.97 and 0.89) for temperature and relative humidity, and moderate (R = 0.68) for wind speed, while wind direction has a weak correlation (R = 0.58). The mean bias error (MBE) reveals a slight overestimation in temperature (1.02 °C), with a higher overestimation of about 25° for wind direction. Conversely, the model underestimates both relative humidity and wind speed, with negative biases of -5.76% and -0.15 m/s respectively. The Mean Absolute Error (MAE) is lowest for temperature (1.3 °C), moderate for relative humidity (6.27%), and larger values for wind speed and direction (1.55 m/s and 48.77°, respectively).

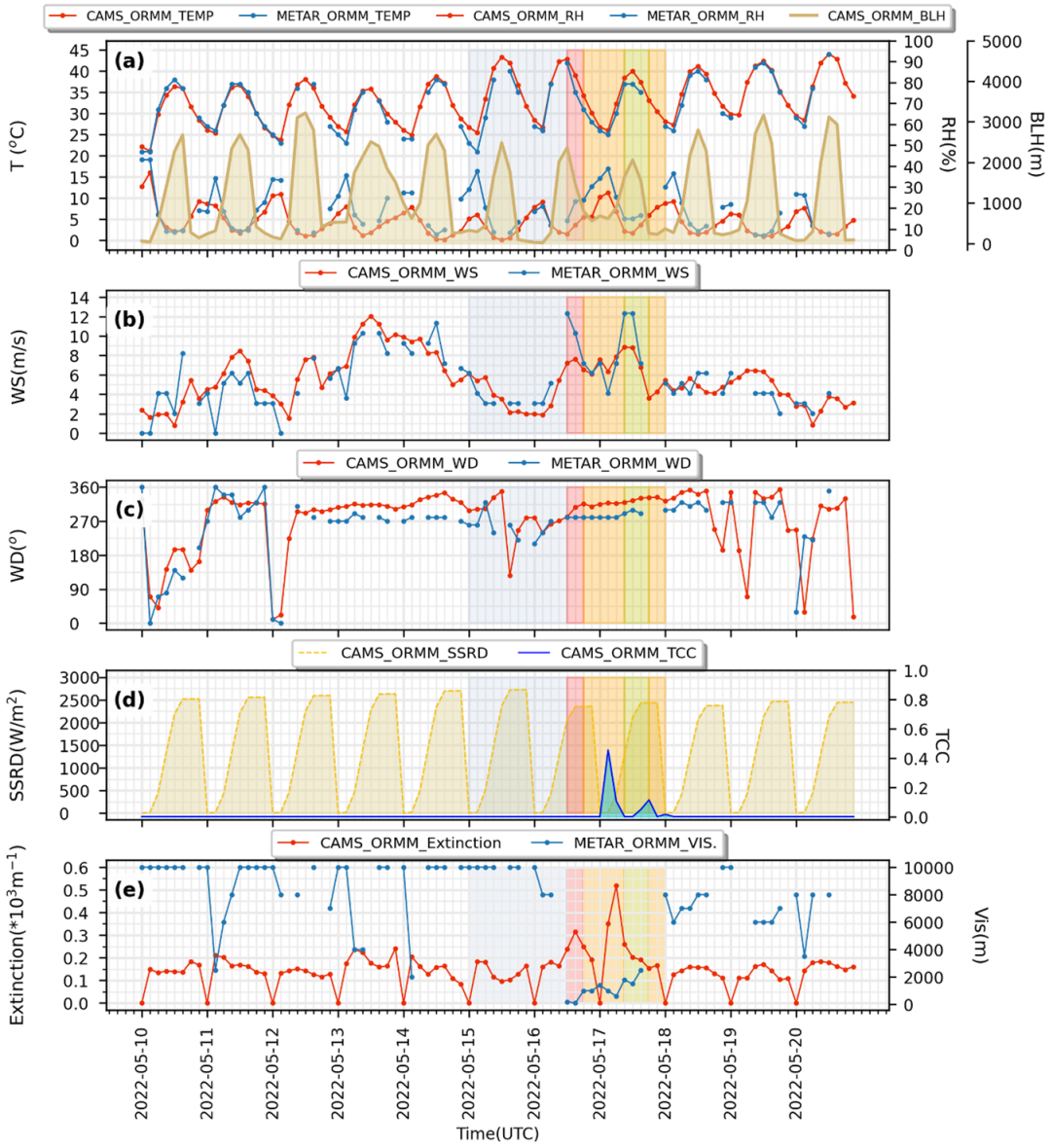

Figure 4. Time series of the meteorological elements acquired from CAMS and METAR data for Basrah (ORMM) station, shaded colors represent the weather conditions where the light blue shaded color represents the before dust event interval, the light reddish shaded color represents dust storm, orange shaded color represents widespread dust and dark yellow shaded color represents blowing widespread dust

Table 2. Statistical metrics of CAMS and METAR data including (MBE, MAE, and R)

Meteorological Variables	MBE	MAE	R
TEMP(°C)	1.016	1.299	0.971
RH (%)	-5.76	6.265	0.89
WS (m/s)	-0.148	1.554	0.68
WD (°)	25.542	48.769	0.584

Figure 5 visually supports the previous finding, which presents scatter plots, regression lines, and the coefficient of determination R^2 for the four variables. Figure 5a reveals a good agreement between both modeled and observed temperature (tight clustering of data around the regression line). Figure 5b shows more spread points around the regression line for relative humidity compared to temperature particularly for RH> 40%, highlighting the underestimation tendency for higher values of RH. As for wind speed in Figure 5c, the variability is higher (more spread points) with underestimation at higher speeds and overestimation at lower ones, indicating a moderate performance. Figure 5d exhibits the most dispersed pattern, with poor alignment between modeled and observed data, confirming low reliability in simulating wind direction.

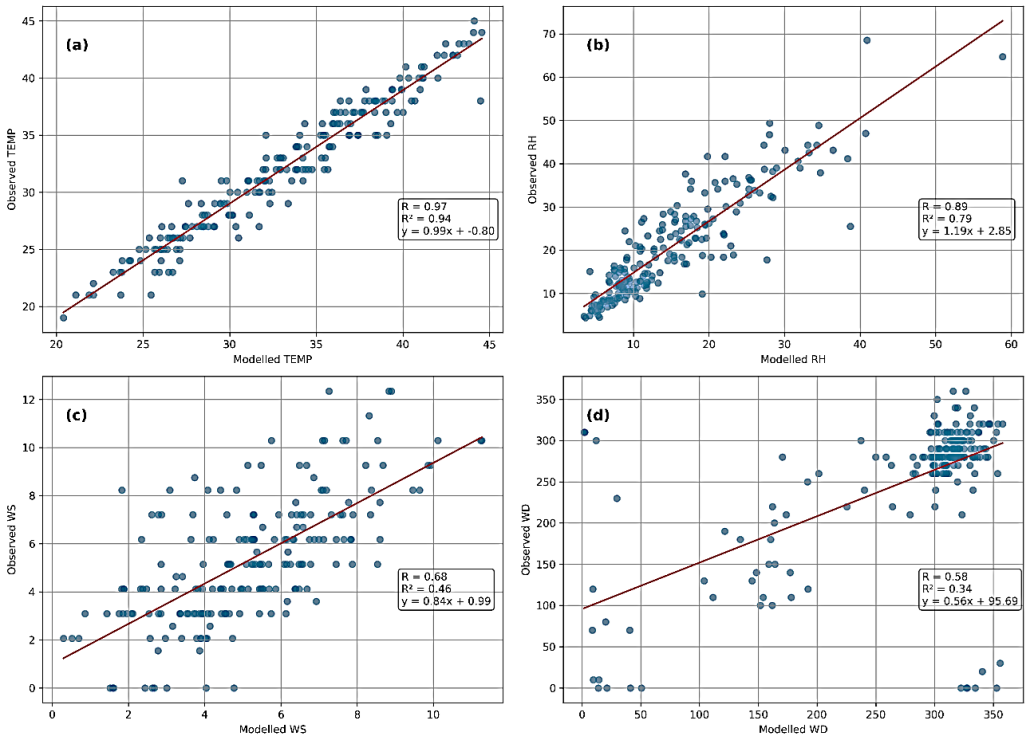

Figure 5. Scatter plots with regression lines comparing CAMS model and METAR observations at Basrah (ORMM) station, (a) for temperature, (b) for relative humidity, (c) for wind speed, and (d) for wind direction

CONCLUSION

In this study, a synoptic analysis was conducted to investigate the weather system behind the mid-May severe dust event that occurred in 2022, affecting the Middle East. Also examined were the variations of meteorological factors during the dust event at Basrah station in southern Iraq. ECMWF-CAMS data for global atmospheric composition forecasts, METAR data, and Dust RGB images of MSG-SEVIRI were used. The main findings revealed that the dust event was driven by a deep frontal cyclonic system, developed on May 15th, generating dense dust clouds, affecting southern Turkey to northern Saudi Arabia, including Syria, Jordan, and western Iraq. Northwesterly winds carried the dust plume southeastward into central and southern Iraq, including Basrah, where it persisted until the cold front's passage on May 18. The dust plume is simulated well in both CAMS AOD and DOD,

showing high values exceeding 2.5 during the dust event.

During the event, a significant decrease was observed at Basrah station in visibility, temperature, and surface solar radiation. Meanwhile, high wind speed, extinction coefficient, and elevation in humidity levels were observed. Also, lower boundary layer height BLH during the day hours, and higher BLH during late evening to early morning hours, reflecting diurnal atmospheric dynamics. A statistical evaluation of CAMS data against METAR observations for May demonstrated strong agreement for temperature and relative humidity, moderate alignment for wind speed, and weak correlation for wind direction. The model tended to slightly overestimate temperature and significantly overestimate wind direction while underestimating relative humidity and wind speed. Errors were generally low for temperature, moderate for relative humidity, and higher for wind speed and direction.

SUPPLEMENTARY MATERIAL

None.

AUTHOR CONTRIBUTIONS

Sama K. Al-Dabbagh: Conceptualization, investigation, methodology, software, data curation, data analysis and interpretation, validation, visualization, writing, review and editing.

FUNDING

This research received no external funding.

DATA AVAILABILITY STATEMENT

All data used are public at:
1. Global Atmospheric Composition Forecasts from Copernicus Atmosphere Monitoring Service (CAMS) https://ads.atmosphere.copernicus.eu/datasets/cams-global-atmospheric-composition-forecasts?tab=overview,
2. METAR data https://mesonet.agron.iastate.edu/request/download.phtml,
3. Dust RGB images https://navigator.eumetsat.int/product/EO:EUM:DAT:MSG:DUST.

ACKNOWLEDGMENTS

The author wishes to acknowledge the editors and reviewers of this manuscript, the use of ECMWF Copernicus Atmosphere Monitoring Service (CAMS) data, EUMETSAT for the provision of METEOSAT RGB imagery, and Iowa Environmental Mesonet (IEM) for providing METAR data.

CONFLICTS OF INTEREST

The author declares no conflicts of interest.

REFERENCES

[1] P. Knippertz and J.-B. W. Stuut, *Mineral dust: A key player in the Earth system*. Springer Netherlands, 2014, isbn: 9789401789783. doi: 10.1007/978-94-017-8978-3.

[2] C. Opp, M. Groll, H. Abbasi, and M. A. Foroushani, "Causes and effects of sand and dust storms: What has past research taught us? A survey," *Journal of Risk and Financial Management*, vol. 14, no. 7, p. 326, 2021. doi: 10.3390/jrfm14070326.

[3] M. C. Thomson, I. Jeanne, and M. Djingarey, "Dust and epidemic meningitis in the Sahel: A public health and operational research perspective," *IOP Conference Series: Earth and Environmental Science*, vol. 7, p. 012 017, Mar. 2009. doi: 10.1088/1755-1307/7/1/012017.

[4] R. Al Nadhairi, M. Al Kalbani, S. Al Khazami, M. Al Hashmi, S. Al Zadai, Y. Al-Rumhi, and K. M. Al-Kindi, "Air quality and health risk assessment during Middle Eastern dust storms: A study of particulate matter," *Air Quality, Atmosphere & Health*, vol. 18, no. 2, pp. 587–603, 2024. doi: 10.1007/s11869-024-01662-8.

[5] T. Li, A. J. Cohen, M. Krzyzanowski, C. Zhang, S. Gumy, P. Mudu, P. Pant, Q. Liu, H. Kan, S. Tong, S. Chen, U. Kang, S. Basart, N. E. Touré, A. Al-Hemoud, Y. Rudich, A. Tobias, X. Querol, K. Khomsi, F. Samara, M. Hashizume, M. Stafoggia, M. Malkawi, S. Wang, M. Zhou, X. Shi, G. Jiang, and H. Shen, "Sand and dust storms: A growing global health threat calls for international health studies to support policy action," *The Lancet Planetary Health*, vol. 9, no. 1, pp. E34–E40, 2025. doi: 10.1016/s2542-5196(24)00308-5.

[6] A. S. Goudie and N. J. Middleton, *Desert dust in the global system*. Springer Berlin Heidelberg, 2006, isbn: 9783540323549. doi: 10.1007/3-540-32355-4.

[7] M. Kanakidou, S. Myriokefalitakis, and K. Tsigaridis, "Aerosols in atmospheric chemistry and biogeochemical cycles of nutrients," *Environmental Research Letters*, vol. 13, no. 6, p. 063 004, 2018. doi: 10.1088/1748-9326/aabcdb.

[8] D. Rosenfeld, Y. Rudich, and R. Lahav, "Desert dust suppressing precipitation: A possible desertification feedback loop," *Proceedings of the National Academy of Sciences*, vol. 98, no. 11, pp. 5975–5980, 2001. doi: 10.1073/pnas.101122798.

[9] D. Francis, J.-P. Chaboureau, N. Nelli, J. Cuesta, N. Alshamsi, M. Temimi, O. Pauluis, and L. Xue, "Summertime dust storms over the Arabian Peninsula and impacts on radiation, circulation, cloud development and rain," *Atmospheric Research*, vol. 250, p. 105 364, Mar. 2021. doi: 10.1016/j.atmosres.2020.105364.

[10] B. Pan, Y. Wang, Y. Lin, J.-S. Hsieh, M. Lavallee, L. Zhao, and R. Zhang, "Radiative and microphysical impacts of the Saharan dust on two concurrent tropical cyclones: Danielle and Earl (2010)," *Journal of Geophysical Research: Atmospheres*, vol. 129, no. 2, 2024. doi: 10.1029/2023jd039245.

[11] A. R. Baker, O. Laskina, and V. H. Grassian, "Processing and ageing in the atmosphere," in *Mineral Dust*. Springer Netherlands, 2014, pp. 75–92, isbn: 9789401789783. doi: 10.1007/978-94-017-8978-3_4.

[12] C. R. Usher, A. E. Michel, and V. H. Grassian, "Reactions on mineral dust," *Chemical Reviews*, vol. 103, no. 12, pp. 4883–4940, 2003. doi: 10.1021/cr020657y.

[13] J. F. Kok, A. A. Adebiyi, S. Albani, Y. Balkanski, R. Checa-Garcia, M. Chin, P. R. Colarco, D. S. Hamilton, Y. Huang, A. Ito, M. Klose, L. Li, N. M. Mahowald, R. L. Miller, V. Obiso, C. Pérez García-Pando, A. Rocha-Lima, and J. S. Wan, "Contribution of the world's main dust source regions to the global cycle of desert dust," *Atmospheric Chemistry and Physics*, vol. 21, no. 10, pp. 8169–8193, 2021. doi: 10.5194/acp-21-8169-2021.

[14] S. K. Al-Dabbagh, "The use of aerosol optical properties in identification of dust sources in Iraq," *Journal of Physics: Conference Series*, vol. 1660, no. 1, p. 012 049, 2020. doi: 10.1088/1742-6596/1660/1/012049.

[15] P. Ginoux, J. M. Prospero, T. E. Gill, N. C. Hsu, and M. Zhao, "Global-scale attribution of anthropogenic and natural dust sources and their emission rates based on MODIS Deep Blue aerosol products," *Reviews of Geophysics*, vol. 50, no. 3, 2012. doi: 10.1029/2012rg000388.

[16] G. Zittis, M. Almazroui, P. Alpert, P. Ciais, W. Cramer, Y. Dahdal, M. Fnais, D. Francis, P. Hadjinicolaou, F. Howari, A. Jrrar, D. G. Kaskaoutis, M. Kulmala, G. Lazoglou, N. Mihalopoulos, X. Lin, Y. Rudich, J. Sciare, G. Stenchikov, E. Xoplaki, and J. Lelieveld, "Climate change and weather extremes in the Eastern Mediterranean and Middle East," *Reviews of Geophysics*, vol. 60, no. 3, 2022. doi: 10.1029/2021rg000762.

[17] X. Wang and C. Zhang, "Sensitivity of soil dust emissions to driving factor variability in earth's main drylands," *Geoderma*, vol. 445, p. 116 876, May 2024. doi: 10.1016/j.geoderma.2024.116876.

[18] A. Rocha-Lima, P. R. Colarco, A. S. Darmenov, E. P. Nowottnick, A. M. da Silva, and L. D. Oman, "Investigation of observed dust trends over the Middle East region in NASA Goddard Earth Observing System (GEOS) model simulations," *Atmospheric Chemistry and Physics*, vol. 24, no. 4, pp. 2443–2464, 2024. doi: 10.5194/acp-24-2443-2024.

[19] M. Hamidi, M. R. Kavianpour, and Y. Shao, "Synoptic analysis of dust storms in the Middle East," *Asia-Pacific Journal of Atmospheric Sciences*, vol. 49, no. 3, pp. 279–286, 2013. doi: 10.1007/s13143-013-0027-9.

[20] Y. Shao, *Physics and modelling of wind erosion*. Springer Netherlands, 2008, isbn: 9781402088957. doi: 10.1007/978-1-4020-8895-7.

[21] D. Francis, R. Fonseca, N. Nelli, D. Bozkurt, J. Cuesta, and E. Bosc, "On the Middle East's severe dust storms in spring 2022: Triggers and impacts," *Atmospheric Environment*, vol. 296, p. 119 539, Mar. 2023. doi: 10.1016/j.atmosenv.2022.119539.

[22] N. H. Hamzeh, S. Karami, D. G. Kaskaoutis, I. Tegen, M. Moradi, and C. Opp, "Atmospheric dynamics and numerical simulations of six frontal dust storms in the Middle East requestegion," *Atmosphere*, vol. 12, no. 1, p. 125, 2021. doi: 10.3390/atmos12010125.

[23] S. Karami, D. G. Kaskaoutis, S. S. Kashani, M. Rahnama, and A. Rashki, "Evaluation of nine operational models in forecasting different types of synoptic dust events in the Middle East," *Geosciences*, vol. 11, no. 11, p. 458, 2021. doi: 10.3390/geosciences11110458.

[24] A. R. S. Abadi, N. H. Hamzeh, M. Chel Gee Ooi, S. S.-K. Kong, and C. Opp, "Investigation of two severe shamal dust storms and the highest dust frequencies in the South and Southwest of Iran," *Atmosphere*, vol. 13, no. 12, p. 1990, 2022. doi: 10.3390/atmos13121990.

[25] S. Tabarestani, G. Kamali, M. Vazifedoust, and S. Sehat Kashani, "Spectral and synoptic analysis of Haboob in Tehran, Iran," *Meteorology and Atmospheric Physics*, vol. 133, no. 4, pp. 1029–1040, 2021. doi: 10.1007/s00703-021-00790-5.

[26] S. Karami, D. G. Kaskaoutis, Z. Ghassabi, and S. Khansalari, "Investigation and model simulation of dry and moist (haboob) convective dust storms in Yazd Province, central Iranian plateau," *Arabian Journal of Geosciences*, vol. 16, no. 4, 2023. doi: 10.1007/s12517-023-11338-9.

[27] R. Papi, S. Attarchi, A. Darvishi Boloorani, and N. Neysani Samany, "Characterization of hydrologic sand and dust storm sources in the Middle East," *Sustainability*, vol. 14, no. 22, p. 15 352, 2022. doi: 10.3390/su142215352.

[28] M. F. Al-Zuhairi and J. H. Kadhum, "Spatiotemporal distribution of the Aura-OMI aerosol index and dust storm case studies over Iraq," *Arabian Journal of Geosciences*, vol. 14, no. 10, p. 909, 2021. doi: 10.1007/s12517-021-07276-z.

[29] C. Fountoukis, H. Harshvardhan, I. Gladich, L. Ackermann, and M. A. Ayoub, "Anatomy of a Severe Dust Storm in the Middle East: Impacts on Aerosol Optical Properties and Radiation Budget," *Aerosol and Air Quality Research*, vol. 20, no. 1, pp. 155–165, 2020. doi: 10.4209/aaqr.2019.04.0165.

[30] S. Basart, C. Pérez, S. Nickovic, E. Cuevas, and J. m. Baldasano, "Development and evaluation of the BSC-DREAM8b dust regional model over Northern Africa, the Mediterranean and the Middle East," *Tellus B: Chemical and Physical Meteorology*, vol. 64, no. 1, p. 18 539, 2012. doi: 10.3402/tellusb.v64i0.18539.

[31] S. K. Mohammed, N. M. A. Fatla, and S. A. A. Wahab, "Numerical simulation of dust event during (1-6) June 2012 using BSC-DREAM8b dust regional model over West Asia, a case study," *IOSR Journal of Environmental Science, Toxicology and Food Technology*, vol. 9, no. 12, pp. 63–78, 2015. doi: 10.9790/2402-091226378.

[32] H. Cao, F. Amiraslani, J. Liu, and N. Zhou, "Identification of dust storm source areas in West Asia using multiple environmental datasets," *Science of The Total Environment*, vol. 502, pp. 224–235, Jan. 2015. doi: 10.1016/j.scitotenv.2014.09.025.

[33] A. S. Alzaid, I. Anil, and O. Aga, "Simulation and assessment of episodic dust storms in Eastern Saudi Arabia using HYSPLIT trajectory model and satellite observations," *Atmosphere*, vol. 15, no. 12, p. 1515, 2024. doi: 10.3390/atmos15121515.

[34] J. E. Oliver, *Encyclopedia of world climatology*. Springer Netherlands, 2005, p. 854, isbn: 9781402032660. doi: 10.1007/1-4020-3266-8.

[35] S. Rémy, Z. Kipling, V. Huijnen, J. Flemming, P. Nabat, M. Michou, M. Ades, R. Engelen, and V.-H. Peuch, "Description and evaluation of the tropospheric aerosol scheme in the Integrated Forecasting System (IFS-AER, cycle 47R1) of ECMWF," *Geoscientific Model Development*, vol. 15, no. 12, pp. 4881–4912, 2022. doi: 10.5194/gmd-15-4881-2022.

[36] U. Schulzweida, "CDO User Guide," en, version 2.3.0, Oct. 2023. doi: 10.5281/ZENODO.10020800.

[37] Iowa Environmental Mesonet, *IEM :: Download Daily Summary Data*. [Online]. Available: https://mesonet.agron.iastate.edu/request/daily.phtml (visited on 06/15/2025).

[38] *Aerodrome reports and forecasts: A users' handbook to the codes*. World Meteorological Organization, 2022, p. 43, isbn: 978-92-63-10782-4. [Online]. Available: https://library.wmo.int/idurl/4/30224.

[39] H. Brindley, P. Knippertz, C. Ryder, and I. Ashpole, "A critical evaluation of the ability of the Spinning Enhanced Visible and Infrared Imager (SEVIRI) thermal infrared red-green-blue rendering to identify dust events: Theoretical analysis," *Journal of Geophysical Research: Atmospheres*, vol. 117, no. D7, 2012. doi: 10.1029/2011jd017326.

[40] P. Broomandi, D. Galán-Madruga, A. Satyanaga, M. Hamidi, D. G. Ledari, A. Fathian, R. Sarvestan, N. Janatian, A. Jahanbakhshi, M. Bagheri, F. Karaca, A. Al-Dousari, and J. R. Kim, "Variability of Middle East springtime dust events between 2011 and 2022," *Air Quality, Atmosphere & Health*, vol. 17, no. 6, pp. 1341–1360, 2024. doi: 10.1007/s11869-024-01510-9.

[41] NASA moderate resolution imaging spectroradiometer, *May 17, 2022 - Massive Middle East Dust Storm*. [Online]. Available: https://modis.gsfc.nasa.gov/gallery/individual.php?db_date=2022-05-17 (visited on 06/15/2025).